Journal of Computer-Aided Molecular Design, **15:** 1085–1104, 2001.
KLUWER/ESCOM

Molecular modeling of interactions of the non-peptide antagonist YM087 with the human vasopressin V1a, V2 receptors and with oxytocin receptors.

Artur Giełdoń, Rajmund Kaźmierkiewicz, Rafał Ślusarz & Jerzy Ciarkowski*
Faculty of Chemistry, University of Gdansk, Sobieskiego 18, 80-952 Gdańsk, Poland

Received 27 April 2000; accepted 28 February 2002

Key words: amber, AutoDock, GPCR receptor/bioligand interaction, molecular dynamics, OT/VP receptors, simulated annealing, YM087

Summary

The nonapeptide hormones arginine vasopressin (CYFQNCPRG-NH_2, AVP) and oxytocin (CYIQNCPLG-NH_2, OT), control many essential functions in mammals. Their main activities include the urine concentration (via stimulation of AVP V2 receptors, V2R, in the kidneys), blood pressure regulation (via stimulation of vascular V1a AVP receptors, V1aR), ACTH control (via stimulation of V1b receptors, V1bR, in the pituitary) and labor and lactation control (via stimulation of OT receptors, OTR, in the uterus and nipples, respectively). All four receptor subtypes belong to the GTP-binding (G) protein-coupled receptor (GPCR) family. This work consists of docking of YM087, a potent non-peptide V1aR and V2R – but not OTR – antagonist, into the receptor models based on relatively new theoretical templates of rhodopsin (RD) and opiate receptors, proposed by Mosberg et al. (Univ. of Michigan, Ann Arbor, USA). It is simultaneously demonstrated that this RD template satisfactorily compares with the first historical GPCR structure of bovine rhodopsin (Palczewski et al., 2000) and that homology-modeling of V2R, V1aR and OTR using opiate receptors as templates is rational, based on relatively high (20–60%) sequence homology among the set of 4 neurophyseal and 4 opiate receptors. YM087 was computer-docked to V1aR, V2R and OTR using the AutoDock (Olson et al., Scripps Research Institute, La Jolla, USA) and subsequently relaxed using restrained simulated annealing and molecular dynamics, as implemented in AMBER program (Kollman et al., University of California, San Francisco, USA). From about 80 diverse configurations, sampled for each of the three ligand/receptor systems, 3 best energy-relaxed complexes were selected for mutual comparisons. Similar docking modes were found for the YM087/V1aR and YM087/V2R complexes, diverse from those of the YM087/OTR complexes, in agreement with the molecular affinity data.

Introduction

The nonapeptide neurohypophyseal hormones oxytocin (CYIQNCPLG-NH_2, OT) and arginine vasopressin (CYFQNCPRG-NH_2, AVP) control many essential functions in mammals via the transmembrane signal transduction path involving GTP-binding (G) protein-coupled receptor (GPCR) and G protein. Their most important – although not unique – actions include the urine concentration (antidiuretic effect), by stimulation of AVP V2 receptors (V2R) in the kidney; blood pressure regulation, by stimulation of vascular V1a AVP receptors (V1aR); ACTH control, by stimulation of V1b receptors (V1bR) in the pituitary; and labor and lactation control, by stimulation of OT receptors (OTR) in the uterus and nipples, respectively. AVP is also involved in many other physiological functions like platelet aggregation, cell proliferation, liver metabolism (e.g. glycogenolysis) [1]. In addition, both AVP and OT are involved in the central nervous system in interneuronal communication and behavioral functions like feeding, memory, thermoreg-

*To whom correspondence should be addressed. E-mail: jurek@chemik.chem.univ.gda.pl

ulation, adaptation and sexual behavior [2]. V2Rs are positively coupled via G_s proteins to adenylyl cyclase and play a major role in the antidiuretic response, while V1aR, V1bR and OTR mediate via $G_{q/11}$ proteins the phospholipase Cβ activation and cytosolic calcium mobilization. Hence, malfunctions of any of the central or peripheral physiological actions (receptors) of both OT and AVP cause pathologies like e.g. certain forms of hypertension (V1aR), coronary vasoconstriction and congestive heart failure (V1aR), edema and/or hyponatremia (V2R), premature labor (OTR and, likely, V1aR). Consequently, there is a great demand for powerful non-peptide agonists and antagonists of the respective receptors, characterized by good selectivity and bioavailability indices. Recent decade has marked a turning point with the design and use of small-molecular *nonpeptide* AVP and OT antagonists [3], which commenced the era of the second-generation ligands for AVP and OT receptors, characterized by good oral availability. They seem to have all benefits of the first-generation *peptide* agonists and antagonists, being at the same time devoid of their greatest disadvantage, i.e. oral non-availability. The first-generation ligands, based on their parent hormones [4], although have scored a great value in pharmacology, have had a very limited value in therapy, as readily metabolizable and thus orally ineffective drugs.

Among the most promising second-generation neurophyseal ligands seem to be SR 49059 [5] and OPC-21268 [6] as orally available selective V1aR antagonists and SR 121463A [7] and OPC-31260 [8] as orally available selective V2R antagonists, L-372,662 as orally available selective OTR antagonist [9], and YM087 (conivaptan hydrocholoride) as orally effective mixed V1aR/V2R antagonist [10], seemingly promising in congestive heart failure [11, 12], see Figure 1. They all have good [6,8] or excellent [5,7,9,10,11,12] pharmaceutical indices regarding their expected biological effect, bioavailability, safety and tolerance, and all of them are undergoing clinical trials.

Our interest in computer-aided drug design seems of particular potential regarding GPCRs, as these receptors, according to recent estimates, are targeted by up to 60% of all drugs in use [13]. However, GPCRs (also termed serpentine or heptahelical transmembrane, 7TM, receptors), as integral membrane proteins, are very reluctant to crystallization and structural analysis. Thus, being the largest family of homologous proteins, represented by over 2000 sequences described, they are – paradoxically – quite poorly known and understood. Yet, it is widely accepted a view that GPCRs share many common structural features [14, 15]. Furthermore, it is proved that their intimate functional partners, the G proteins, do indeed share structural elements among themselves, even if they are involved in diverse physiological actions [14–18], induced by varied primary signals. Indeed, despite an exceptional diversity in primary signals among GPCRs (ranging from photons, neurotransmitters, peptide hormones, nucleosides and nucleotides, eicosanoids, metal ions, through glycoprotein hormones [15]), all receptors utilize the same transduction mechanism, implicating a cytosolic heterotrimeric GTP-binding (G) protein in mediation between a GPCR and an intracellular target effector. The latter are various enzymes or ion channels, generating secondary intracellular signals, virtually controlling all cell activities [14, 15, 17, 18]. The structural homology among GPCRs consists of a common heptahelical transmembrane domain (7TM), also exhibiting up to $\sim 20\%$ sequence homology [19, 20].

Until very recently [21], no details on the GPCR architecture had been known at the atomic resolution level, thus GPCRs were only available from molecular modeling, typically coupling a low resolution (6 Å) structure of rhodopsin (RD) - the only GPCR of known structure [21–23] – with a multi-sequence analysis [19, 20]. One of the most rational strategies of the GPCR modeling using this scheme [20, 24, 25] consists of a multi-sequence alignment of some 200–500 representative GPCRs, resulting in a statistical probe for distributions of polar/non-polar and conservative/non-conservative residues, thus allowing a choice of the putative TM1-TM7 helices along the sequence. Subsequently, TM1-TM7 are threaded onto the low-resolution structure of rhodopsin [23], so that most of the experimental constraints are met [20, 24]. The result is then refined via constrained simulated annealing (CSA) to the self-consistency of 1.67 Å [24]. The 7TM template [20] or even an automated GPCR-modeling server, based on this scheme, are available via Internet [25]. The resulting GPCR template, even if chiefly applying to rhodopsin, provides for a good start for 7TM models of other receptors, given the sequence homologies among various GPCR subfamilies [26]. An alternative, *ab initio*-like approach recently proposed by Mosberg et al. [27], also uses multi-sequence alignment for the choice of the 7TM helices, followed by a distance-geometry optimization applied simultaneously to 430 GPCR sequences. First, puta-

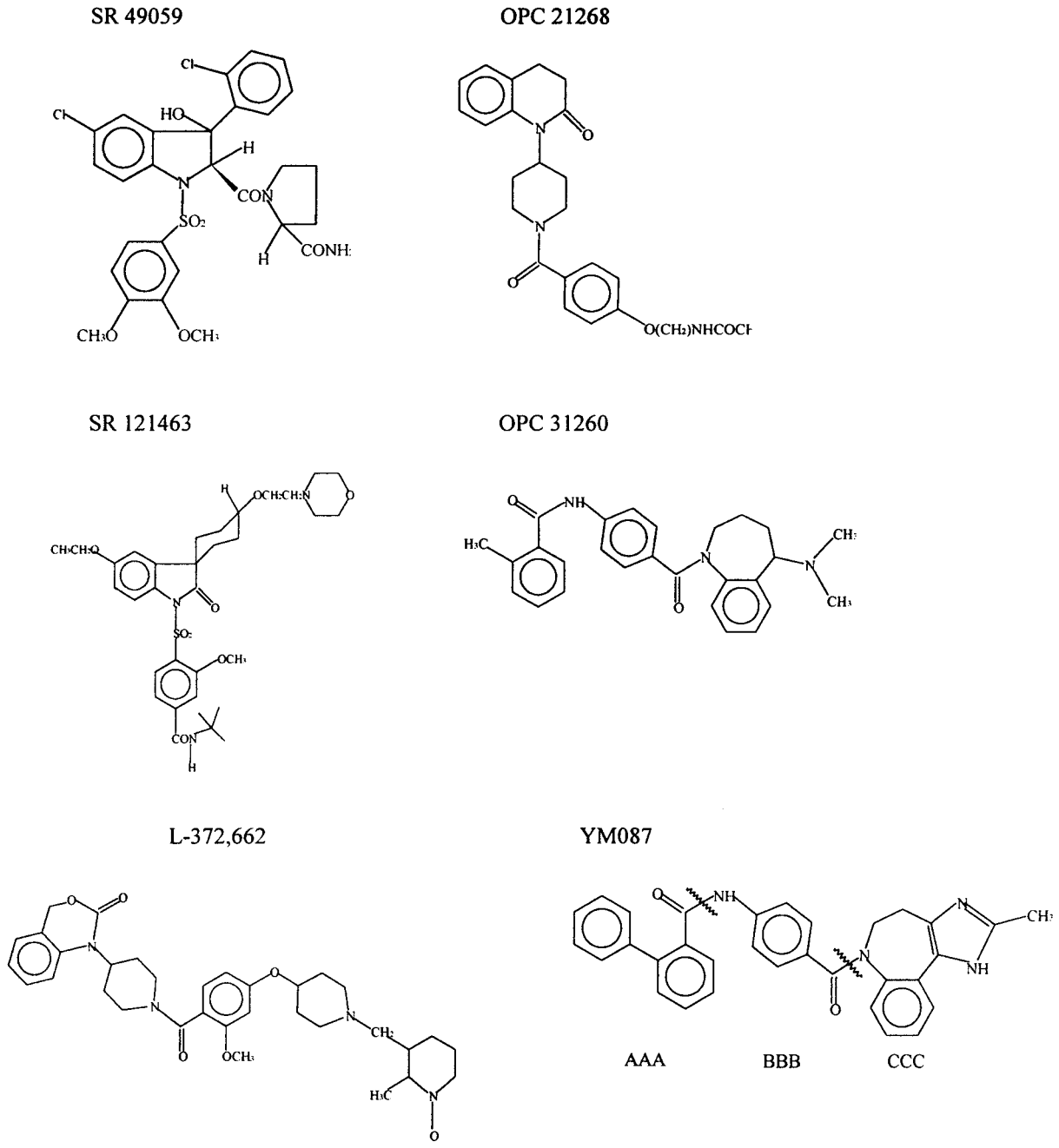

Figure 1. Molecular topologies of nonpeptide V1aR (SR 49059, OPC-21268, YM087), V2R (SR 121463A, OPC-31260, YM087) and OTR (L-373,662) antagonists. The subdivision of YM087 for parameterization in AMBER [30] (see Methods) is indicated.

tive hydrogen bonds between polar/charged residues within the GPCR interior are singled out. Subsequently, they are used collectively and simultaneously for many overlapping GPCRs as constraints in the iterative distance-geometry procedure, aimed at the optimization of an averaged 7TM bundle, typical of all 430 sequences.

We have checked that the 7TM bundles resulting from the threading [20] and the *ab initio*-like procedures [28] are mutually convergent to 3.3 Å. Given all other the same, the latter method was more attractive to us as it provided more complete GPCR models, including also the extra-membrane loops, as exemplified in the opiate receptor models [28]. Furthermore, after the recent landmark work describing a high-resolution crystal structure of RD [21], we found that the theoretical RD-model chosen by us [27] compares very favorably with the experimental structure, see Figure 2.

In addition to a very good fit (root-mean-square deviation, rms, for the bundles equals 1.71 Å), in the theoretical model of Pogosheva et al. [27] most of the experimentally observed inter-helical links and relationships are predicted. For instance, a net of hydrogen bonds among conservative N55, D83, A299 and N302, holding together the TM1, TM2 and TM7 helices, was in the theoretical model not only predicted to exist but also in nearly the same mutual architectures of the respective amino acids, as in the experimental structure, see Figure 2. A majority of other inter-helical links, involving additional conservative amino acids, were also properly predicted, see Figure 2. The only significant difference regarded TM7 Y306 having its side chain flipped to $\chi_1 \approx 60°$, contrary to $\chi_1 \approx 180°$ in the experimental structure, thus preventing in the model (but not precluding, given the Y306 side-chain rotates) the TM7 Y306 – TM2 N73 hydrogen-bond link [21], see Figure 2. The only definite mismatch between the model and the experimental structure consisted of not involving in the former TM4 T160 into another net of hydrogen bonds comprising, apart of T160, conservative TM2 N78, TM3 S127, TM4 W161 and holding TM2 and TM4 together. At this point, it is worth mentioning, that TM1, TM2, TM3 and TM7 of the model fit almost perfectly those of the real structure. Some not too significant shift consists TM4s, resulting in the T160 feature mentioned above, while theoretical and experimental TM5s fork away towards extracellular surface, the latter further away of the bundle center, to reach some 5–6 Å disagreement at their N-termini. Finally, TM6 in the model is by $\sim$4 Å, i.e. approximately by a helical pitch shifted extracellular, relative to its experimental counterpart. Despite this seemingly most critical difference, another TM3-TM6 link near the cytosol surface, involving E134 and R135 of TM3 conservative ERY sequence and conservative TM6 E247 and T251, is reproduced in the model, although with appreciably different architecture, see Figure 2. Finally, the 11-*cis*-retinals make extracellular convex arcs, parallel to each other and mutually coiled clockwise by some 90° along their full lengths. Thus, the NZ-imine K296 nitrogens start separated by 4.44 Å roughly parallel to the bilayer normal, with the experimental one more extracellular, then the polyene chains get closer to each other at C13 through C9 coiling center (3.55 Å and 3.49 Å, respectively), to diverge again to $\sim$4.4 Å at the β-ionon rings. Both rings end nearly between their respective TM5 and TM6 helices at approximately common high along the bilayer normal, in accord with their coiling: the experimental one apparently closer to TM5 while the theoretical one closer to TM6, see Figure 2. This feature is compatible with the experimental TM5 leaning away of the bundle by some 5 Å at its N-terminus relative to the theoretical one, see above. The only noticeable difference regards the β-ionon orientations: the experimental one is placed roughly parallel to the bilayer normal while the theoretical one – perpendicular to it, see Figure 2. What mostly counts in this context, however, is that the retinals interact with the equivalent sets of opsin amino acid residues [21, 27] in the both models. In summary, the overall similarity of our former choice with the experimental model seemed satisfactory enough to stay with the theoretical model at the moment [27, 28].

A multi-sequence alignment for four human neurophyseal receptors V1aR, V1bR, V2R, and OTR, and three opiate receptors, μ, δ, κ, exhibits sizeable homology (20–60%) among the two receptor groups, hence strongly argues for common structural features between/among the neurophyseal and opiate receptors. Subsequently, the V1aR, V2R, and OTR models are described, based on the '*ab initio*' opiate models given by Pogozheva et al. [28]. Finally, the results of docking of YM087, a mixed V2R/V1aR non-peptide antagonist (using the Autodock program [29]) and subsequent its relaxation via constrained simulated annealing and molecular dynamics (using the AMBER ver. 5.0 program [30]), to/in each of the three receptor models, are presented. Similar docking modes were found for the YM087/V1aR and YM087/V2R

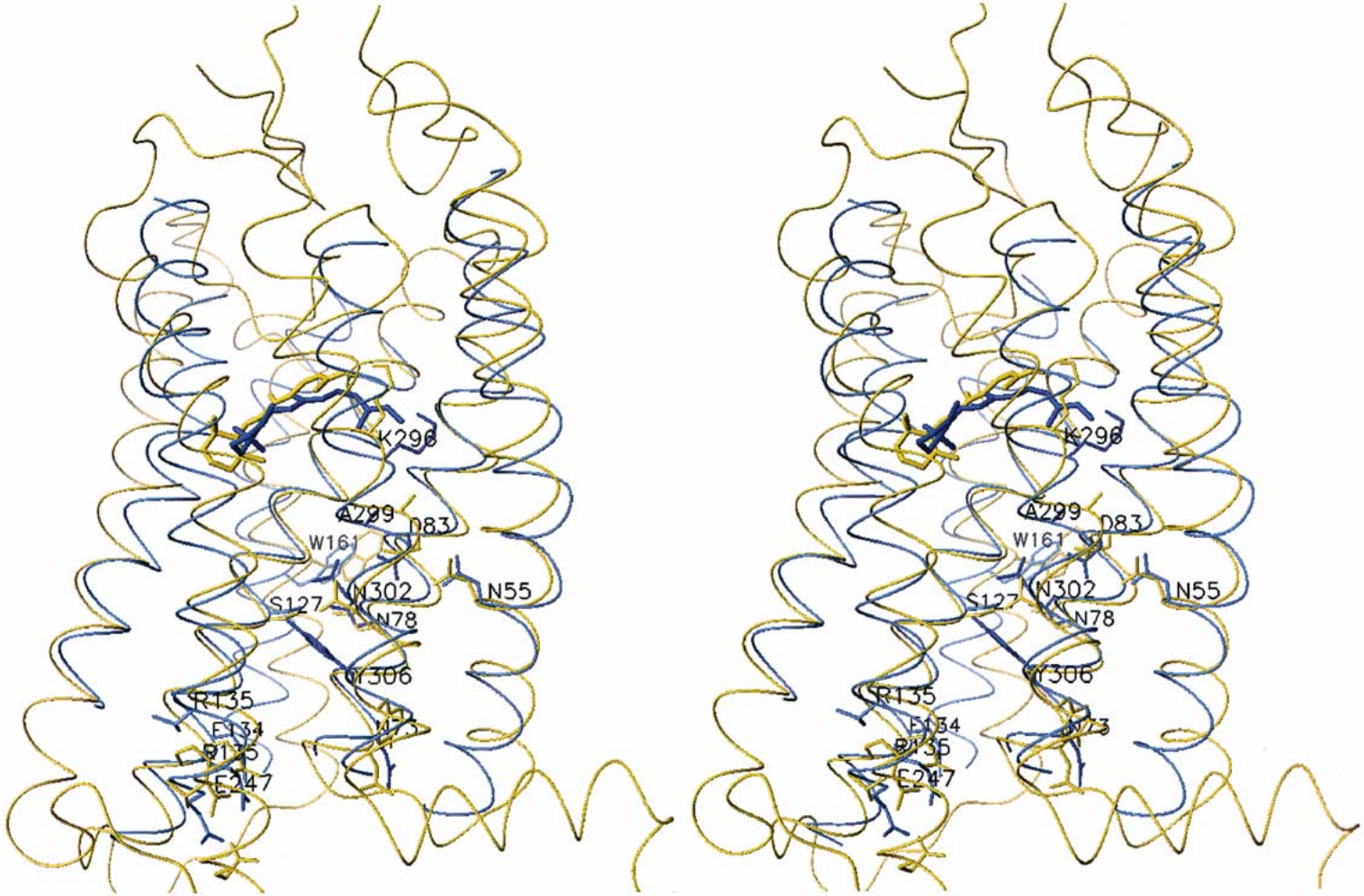

Figure 2. Overlapping RD models: the theoretical one by Pogosheva et al. [27] (cyan) and the experimental structure [21] (gold). Root-mean-square (RMS) deviation within the TM domains equals to 1.71 Å. See the text for details.

complexes, diverse from those of the YM087/OTR complex, in agreement with experimental data.

Methods

V2, V1a and OT receptor models

The incomplete, with intracellular loops 2 and 3 (IL2 and IL3, respectively) missing, human opiate-δ receptor model was obtained due to courtesy of Dr H. Mosberg, University of Michigan, Ann Arbor, Michigan, USA [28]. The multiple sequence alignment, Figure 3, exhibited at least 20% sequence homology between the most dissimilar neurophyseal (V1b) and opiate (κ) receptor. This feature strongly supported likely structural analogies between the two GPCR subfamilies.

Thus, given the TM helices and loops aligned, the starting models of V2R, V1aR and OTR were obtained by imposing respective computer mutations/insertions/deletions on the opiate-δ receptor, using the Biopolymer module within the SYBYL suite of programs [31]. Missing IL2 and IL3 were added using the same module's procedure for homology modeling/loop closure. Although the resulting IL2 and IL3 structures thus obtained were quite fortuitous, incidentally, the mainly α-helical IL3 appeared strikingly similar to the recent OTR [32] and a former α_{1B}-adrenergic receptor [33] models by Fanelli and coworkers. The extracellular N- and the cytosolic C-terminal domains were similarly homology-modeled and attached using the Biopolymer module of SYBYL. Only 10 or 8 N-terminal residues (S24-D33 in V2R, G38-N47, and T28-N35 in OTR) directly preceding TM1, see Figure 3, and only 15 residues (S330-R344 in V2R, G353-N368 in V1aR, G334-A349 in OTR), see Figure 3, directly following TM7 were included in the models. In particular, on the C-terminal side, we took care to include a double Cys sequence, typically appearing 10–12 sites away of the TM7 C-terminus, believed to be palmitoylated in the native state(s) and thus providing a hook-up for a putative IL4 [14, 15, 18, 26]. We modeled these -Cys-Cys- sequences accordingly and oriented the two palmitoyl hydrocarbon chains in parallel to the receptor's TM domains. We disregarded the N-terminal (see above) and the C-terminal non-conserved sequence fragments (G345-S371 in V2R, M369-T418 in V1aR and S350-A389 in OTR), see Figure 3, of variable lengths and obscure function [14, 15, 18, 26]. The putative conservative disulphide, coupling EL1 with EL2 [26], was set manually, resulting in the Cys^{112}-Cys^{192}, Cys^{124}-Cys^{203} and Cys^{112}-Cys^{187} links in V2R, V1aR and OTR, respectively. Thus, obtained receptor models had identical TM backbone architectures due to a strict conservation of the corresponding TM C^{α} positions, yet they differed among themselves in all other aspects, including TM side chains and extra- and intracellular domains. Subsequently, a CSA cycle up to 1000 K, see Figure 4, was applied in vacuo for their efficient relaxation, upon positional constraints imposed on all TM C^{α} carbon positions. Detailed CSA protocol was described elsewhere [34]. Finally, all three receptor models were minimized (2000 cycles in vacuo), with all TM C^{α} carbon positions constrained, using the AMBER 5.0 [30] suite of programs.

Parameterization

All non-standard fragments were parameterized as recommended in the Amber 5.0 manual [30]. The YM087 ligand was split into three 'residues' termed Aaa, Bbb and Ccc, as marked in Figure 1. Since YM087 is stored and administered as hydrochloride [11, 12], this implies the Ccc imidazol to be protonated and respectively charged, as reflected in the parameterization. The palmitoylates, see above, were treated accordingly. The point charges were optimized by fitting them to the *ab initio* molecular electrostatic potentials (6-31G* basis set, GAMESS molecular orbital program package [35]) for several conformations of each new residue, followed by consecutive averaging the charges over all conformations, as recommended in the RESP protocol [36].

Docking YM087 in the receptors

The ligand was docked using the Autodock program, ver. 2.4, of Olson and coworkers [29]. Since the program allows only for one of the docking partners be flexible, the receptor was set to be stiff while YM087 elastic. Briefly, first one has to define an active space confined to an interior of a rectangular prism and comprising the putative cavity allowed to the ligand. In the present case the prism size was 15 Å × 15 Å × 33 Å and comprised both the receptors pocket and the lid composed of the extracellular domains (see below). Having this done, one computes a potential field within the prism, reflecting distribution of the interaction energy of a probe within the host (in our case, with the internal surface of the receptor pocket). This potential is quite crude and includes only Van der Waals and electrostatic energy terms. In the final

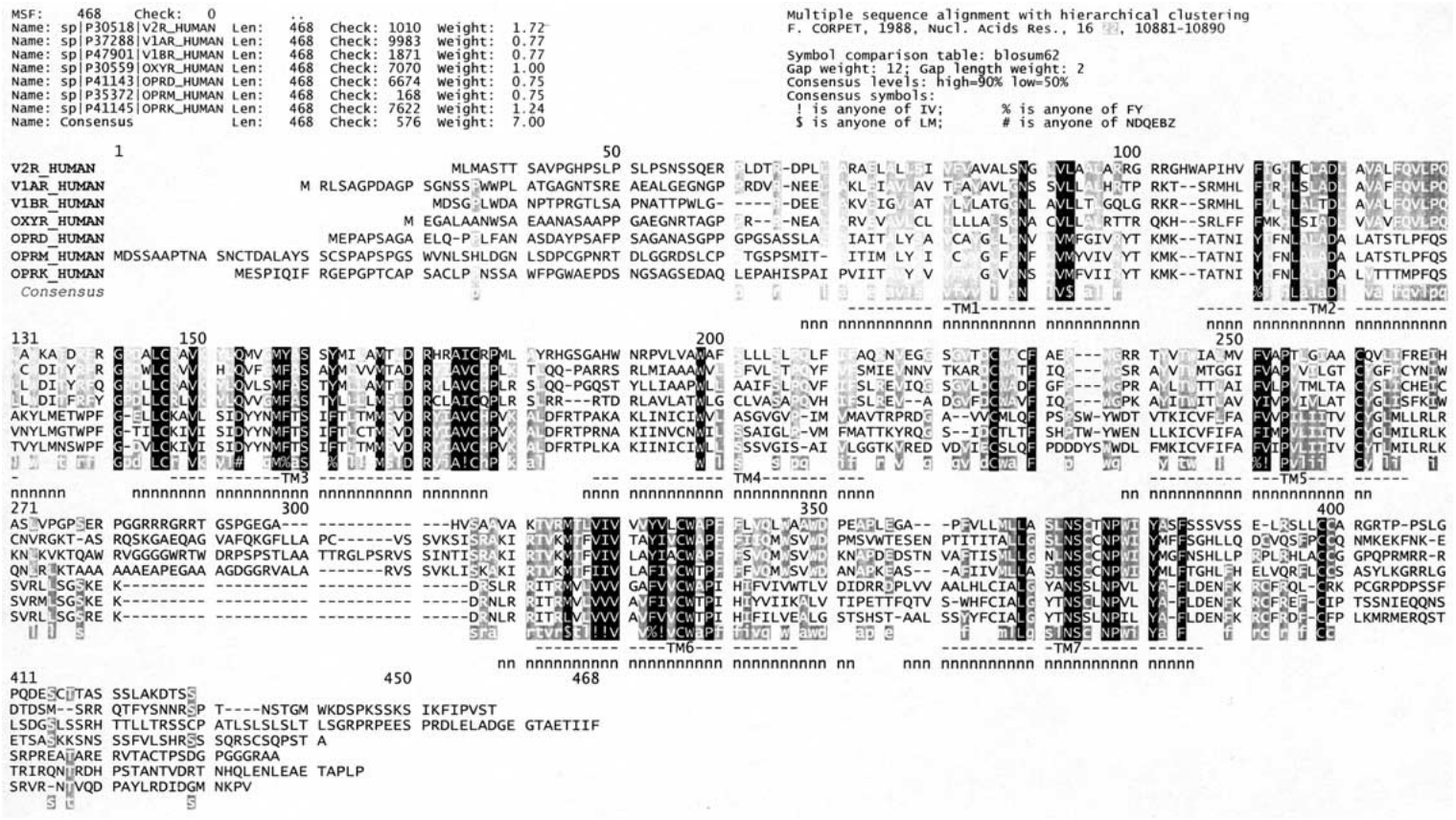

Figure 3. Multiple sequence alignment applied to four human neurophyseal (V2, V1a, V1b and OT) and three human opiate (δ, μ and κ) receptors. The putative TM helices, adopted in this paper from Pogozheva et al. [27,28] are marked 'n'. The TM helices ensuing from the first multisequence GPCR analysis of Baldwin [19] are also given (as TM1-TM7) for reference. The alignment, done using the Multalin program [38], indicates a higher-level similarity black and a lower-level similarity gray. In our models, consistent with that of Pogozheva et al. [27, 28] the helices contributing to the TM bundle consist of the following number residues: TM1-33, TM2-30, TM3-35, TM4-28, TM5-24, TM634 and TM7-28.

step, multiple configurations of the ligand are probed within the prism in the field generated. The resulting initial set of 480–600 receptor-ligand configurations was very crude and required further refinement. To this end, in the first step, all configurations were energy-minimized (2000 cycles in vacuo), with all TM C^{α} carbon positions constrained, using the AMBER 5.0 [30] suite of programs. Subsequently, the receptor-YM087 interaction energy terms were compared and for further refinement only those configurations retained, whose receptor-YM087 interaction energy was $\sim$1000 kcal/mole or less above the absolute minimum. This allowed elimination of all configurations non-repairable by AMBER minimization, e.g. those with mutually stalled or knotted YM087-receptor fragments. In addition, all configurations in which YM087 was oriented with its charged imidazol towards interior of the receptor pocked, were also eliminated. Both criteria combined, typically resulted with $\sim$30 surviving configurations for further refinement. In the second step, a cycle of CSA up to 1000 K, see Figure 4, was applied in vacuo for efficient relaxation of the configurations, upon positional constraints imposed on all TM C^{α} carbon positions. Final configurations were selected whose minimized receptor-ligand interaction energy was $\sim$20 kcal/mole or less above the minimum, including the latter. This resulted in 4, 5 and 8 configurations in OTR, V2R and V1aR, respectively, see Figure 5.

Three selected possibly as simultaneously the most diverse and the lowest-energy ones of each category were taken as starts, see Table 1, for the 500 ps of AMBER 5.0 molecular dynamics in vacuo, with the partial compensation for the environment by setting the dielectric permeability ε equal to 4R. To prevent unfolding and/or whatever perturbations of the TM helices, flat-bottom soft harmonic-wall constraints were imposed onto the φ, ψ and ω peptide angles of the TM amino acid residues, see Figure 2. These constraints, maintained at all times and centered around the ideal helix values had a uniform force constant equal to 40 kcal (mol deg)$^{-1}$ and the torsion angle limits (-115, -81, -47, -13), (-115, -63, -21, -13) and (145, 172, 188, 215) for φ, ψ and ω, respectively. In addition, the positional constraints for all patmitoyl atoms were also maintained at all times. The dynamics were carried out in accord with the following protocols: 1–20 ps – linear heating 0–300 K, with positional TM CA constraints. 20–100 ps – positional TM CA constraints at constant 300 K. 100–160 ps – positional TM CA constraints gradually and simultaneously in each of 7 TM helices released: every two CA N- and C-terminal pairs per every 10 ps at constant 300 K, until complete release at 160 ps. 160–500 ps – Positional-unconstrained (except palmitoyls) dynamics at constant 300 K. Snapshots extracted from/after dynamics/CSA for analysis were energy minimized, see above.

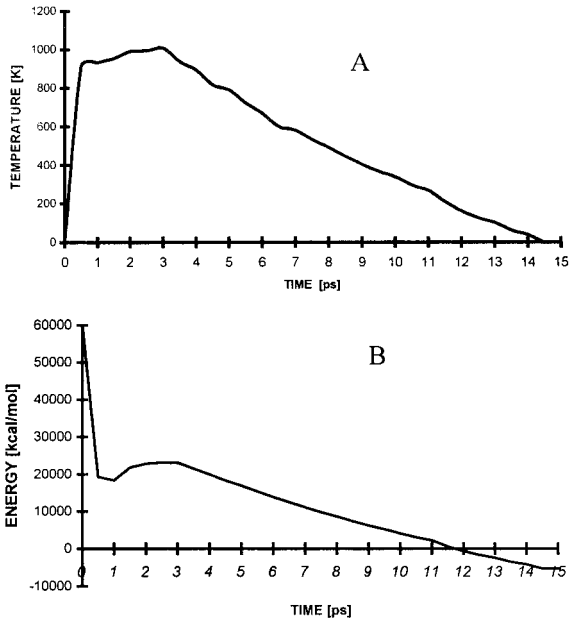

Figure 4. A time-schedule for temperature and energy evolution in a single CSA cycle protocol (for the 1-A YM087-OTR complex as an example).

Hardware and supporting software

Docking and CSA computations were done on SGI Power Challenge 8×R10000, SGI Origin-2000 4×R10000 and/or Sun Enterprise 450 2×UltraSparc-II 300 MHz computers. MD was done on a 4 CPU/node, 32 node, 512MB RAM/node cluster INTEL XEON 700 MHz. The molecular images for presentation were prepared using the MolMol program [37].

Results and discussion

Multiple sequence alignment

In Figure 3 the results of multiple sequence alignment [38] including four human neurophyseal receptors (V2R, V1aR, V1bR and OTR) and four human opiate receptors (δ, μ, κ and χ) are presented. It is

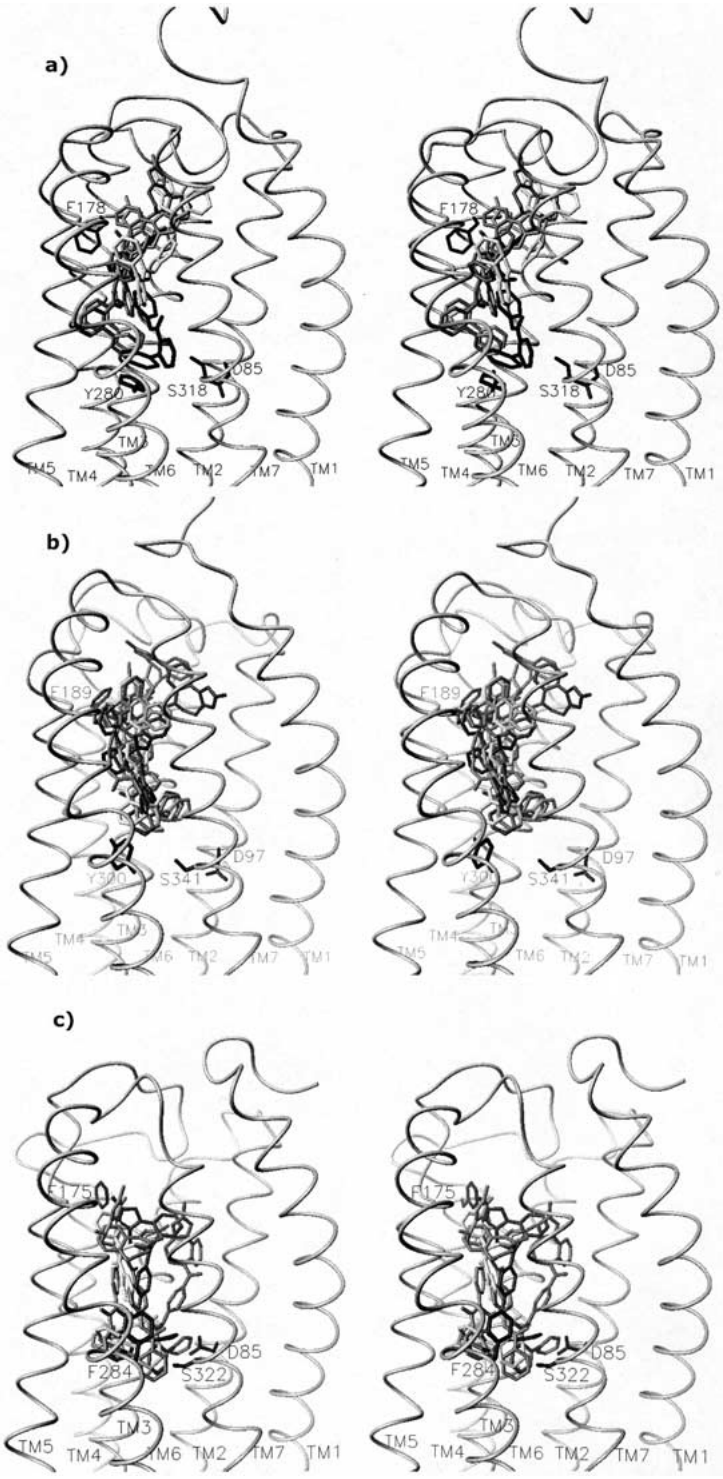

Figure 5. Stereodiagrams of the relaxed YM087 docking modes in A: V2R; B: V1aR; and C: OTR. Only the receptor extracellular halves are exposed. The receptors are shown schematically as their backbone ropes. The overlapping ligands are shown as wireframes. For energies, see Table 1. The following conservative residues in the order (V2R,V1aR,OTR in A,B,C, respectively) have been exposed and labeled for reference: TM2:D(85,97,85); TM4:F(178,189,175); TM6:Y(280,300),F(284); and TM7:S(318,341,322).

Table 1. Interaction energies of the CSA-relaxed and minimized low-energy YM087-receptor complexes[a]. Those selected for MD in each set are marked in bold. Their motional behavior in CSA is also indicated, see alse Figure 5.

V2R			V1aR			OTR		
Code	Energy	Motion	Code	Energy	Motion	Code	Energy	Motion
05	−120.23	m	02	−96.61	vl	**01**	**−62.61**	**s**
06	**−112.73**	**l**	05	−99.13	vl	**06**	**−86.76**	**s**
18	**−115.19**	**l**	**10**	**−104.07**	**l**	**14**	**−78.24**	**s**
26	**−104.23**	**m**	12	−96.62	l	29	−76.48	s
27	−112.40	m	16	−105.80	l			
			18	**−112.73**	**vl**			
			19	−100.28	l			
			20	**−96.92**	**l**			

[a]Energy in Kcal/mol; motion s-small, m-medium, l-large, vl-very large.

seen that there are extensive homologies between the two groups not only within the TM domain (especially within TM3, TM6 and TM7) but also within the extracellular loops 1 and 2, see Figure 3. This feature has substantiated a hypothesis on possible extensive structural analogies between/among the two groups of receptors and validated further homology modeling of the neurophyseal receptors using opiate receptor models as templates.

GPCR models

The 'empty' receptor models based on the dark rhodopsin template [20, 24, 25, 27] seem most suitable for docking antagonists as those tend to freeze the inactive GPCR forms, typical of the former. Thus, assuming sequence alignment validating structural homologies within the TM bundle, it may be worthwhile to analyze in more detail the intra-bundle interactions within 'empty' V1aR, V2R and OTR. In Table 2 the intra-bundle interactions are listed and compared in relaxed energy-minimized V1aRs, modeled using the theoretical model of Pogozheva et al. [28] and the experimental model of Palczewski et al. [21].

First, it is seen, that despite some differences in TM4-TM6 between the model and the experimental structure of RD (see above), the sets of intra-TM bundle interactions in both V1aR models are quite similar and that – quite remarkably – they mainly involve conservative residues. Thus, in both models the helices 1, 2, 3 and 4 are linked by the sets of intra-bundle hydrogen bonds between, respectively, TM1:N69 and TM2:S94 (theoretical template) or proximal D97 (experimental template), D97 and TM3:S138, TM2:H92 and TM4:S138 TM2:H92 and TM4:R168 (via an H_2O or OH^- in the theoretical template) or TM2:H92 and TM4:W175 (via an H_2O or OH^- in experimental template). There are also seen two potential mutually interfering intra-bundle switches in both models. The first polar one, with the pivoting TM3:R148/D147 pair in its center, potentially ranging from TM2:R85 to TM6:T289 (and/or T293, not shown) to TM7:Y348 and the other non-polar one, with the pivoting TM7:Y348 in its center, potentially ranging from TM1:V72 to TM2:M86 to TM3:I142 and R149 to TM6:T289. In addition, there are three sets of extensive non-polar intra-TM bundle interactions, centered around the following clusters of hydrophobic residues: (1) TM6:M292, I296 and TM7:I347, Y348 and F351; (2) TM3:V132, M135, F136, TM4:I131, TM5:T221, I224, F225, TM6:Y300, I301,W30; (3) TM6:W304, F307, F308. The major difference between the two models relies on that that the experiment-based [21] TM-bundle of V1aR is slightly better internally optimized, as seen in its more intense network of interactions than in the former.

In Tables 3 and 4, the lists of similar sets of interactions enable comparisons between our V1a, V2 and OT receptor models, based on the theoretical model of Pogozheva et al. [28]. It is quite clear that, to a large extent, equivalent sets of intra-bundle interactions stabilize 'empty' inactive forms of neurophyseal receptors. Given prevailingly conservative nature of contributing residues, this hypothesis may be extended on the whole Rhodopsin-like GPCR family.

Any GPCR modeled to the RD template [24, 25, 27, 28] has a deep (∼20 Å) cleft on its extracellular side, surrounded by the helices TM3-TM7, with a narrower extension towards TM2. The

Table 2. The matrix of interactions between the conservative residues within the TM bundle of empty V1aR. A: a model based on the theoretical structure [28], B: a model based on the experimental structure [21][a,b,c].

A		TM2		TM3				TM4			TM5		TM6						TM7		
		R85	S94	*F136*	*S138*	*M141*	*M145*	*R168*	I171	W175	I224	F225	*T289*	Y300	*I301*	W304	F307	*F308*	I347	Y348	*F351*
TM1	N69		p																		
	V72																			s2	
TM2	*M86*						h													s2	
	F89					h	h		h												
	H92							p													
	D97				p																
TM3	*V132*			hc																	
	M135			hc								hc		hc		hc					
	F136										hc										
	M141									h											
	I142																			s2	
	M145																			h	
	T146										p										
	D148	s1																			
	R149	s1											s1							s1,s2	
TM5	*T221*			hc																	
	I224			hc																	
	F225													hc	hc						
TM6	T289																			s2	
	M292																		h	h	h
	Y300															hc	hc				
	I301																hc				
	W304																	hc	hc		
	F307																		hc		

Table 2. Continued.

B		TM2			TM3				TM4			TM5		TM6						TM7		
		R85	*M86*	D97	*F136*	*S138*	*M141*	*M145*	*Q162*[d]	I171	W175	I224	F225	*T289*	Y300	*I301*	W304	F307	*F308*	I347	Y348	*F351*
TM1	N69			p																		
	V72																				s2	
TM2	*M86*							h													h,s2	
	F89						h	h		h												
	I90																				h	
	H92										p											
	D97					p																
TM3	*V132*																					
	M135				hc							hc	hc		hc		hc					
	F136											hc	hc									
	M141									hc												
	T146																					
	D148	s1							p													
	R149	s1												s1							s1,s2	
TM5	*T221*				hc																	
	I224				hc																	
	F225														hc	hc						
	V229														hc	hc						
TM6	T289																				s2	
	M292		h																	h	h	h
	I296		h					hc												h	h	
	Y300															hc	hc					
	I301																hc					
	W304																	hc	hc			
	F307																		hc			

[a]Non-conservative residues are written in italic.
[b]h – hydrophobic; p – polar interaction; s1 – R149 switch-1, potentially reaching TM2 R85 (via D148), IL3/TM6 T289 (via water) and TM7 Y348; s2 — Y348 switch-2, potentially reaching TM1 V72, TM3 I142, R137 and TM6 T273.
[c]hc – cluster of hydrophobic residues. The interactions indicated may reconfigure to a noticeable extend, due to flexibility and considerable size (e.g. metionin, aromatics) of the contributing residues.

Table 3. The matrix of interactions between the conservative residues within the TM bundle of empty V2R[a,b,c].

		TM2		TM3			TM4		TM5	TM6						TM7				
		P73	C82	*Y124*	*M129*	*M133*	*R158*	W164	F214	*T269*	Y280	*V281*	W284	F287	*F288*	S318	*C319*	I324	Y325	*F328*
TM1	N55		p														p			
	V58																		s2	
TM2	*I74*					h													s2	
	F77				h	h														
	H80						p													
	D85															p				
TM3	*M120*			hc																
	M123			hc					hc		hc		hc							
	Y124								hc											
	M129							h												
	I130																		s2	
	R137	s1								s1									s1,s2	
TM5	F214										hc	hc								
TM6	*M272*																	h	h	h
	T273																		s2	
	Y280											hc	hc							
	V281												hc							
	W284													hc	hc					
	F287														hc					

[a]Non-conservative residues are written in italic.
[b]h – hydrophobic; p – polar interaction; s1 – R137 switch-1, potentially reaching TM2 P73 C'O, IL3/TM6 T269 and TM7 Y325; s2 – Y325 switch-2, potentially reaching TM1 V58, TM2 I74, TM3 I130, R137 and TM6 T273.
[c]hc – cluster of hydrophobic residues. The interactions indicated may reconfigure to a noticeable extend, due to flexibility and considerable size (e.g. metionin, aromatics) of the contributing residues.

Table 4. The matrix of interactions between the conservative residues within the TM bundle of empty OTR[a,b,c].

		TM2			TM3			TM4		TM5	TM6						TM7				
		H71	*R73*	D85	*F124*	*L129*	*M133*	*R154*	W161	Y209	*T273*	F284	*I285*	W288	F291	*F292*	S322	*C323*	I328	Y329	*F332*
TM1	N57			p														p			
	V60																			s2	
TM2	*L74*						h													s2	
	F77					h	h														
	H80							p	p												
	D85																p				
TM3	*V120*				hc																
	M123				hc					hc		hc		hc							
	F124									hc											
	L129																				
	L130																			s2	
	D136	p	s1																		
	R137		s1								s1									s1,s2	
TM5	Y209											hc	hc								
TM6	*M276*																		h	h	h
	T277																			s2	
	F284												hc	hc							
	I285													hc							
	W288														hc	hc					
	F291															hc					

[a]Non-conservative residues are written in italic.
[b]h – hydrophobic; p – polar interaction; s1 – R137 switch-1, potentially reaching TM2 R73 (via D136), IL3/TM6 T273 and TM7 Y329; s2 – Y329 switch-2, potentially reaching TM1 V60, TM2 L74, TM3 L130, R137 and TM6 T277.
[c]hc – cluster of hydrophobic residues. The interactions indicated may reconfigure to a noticeable extend, due to flexibility and considerable size (e.g. metionin, aromatics) of the contributing residues.

cavity floor is lined mainly with hydrophobic conservative residues (in V2R, V1aR, OTR, respectively) in TM2: P(95,107,95); TM3: M(123,135,123); TM5: V(206,217,208), T(207,218)Y(209); TM6: W(284,304,288), F(287,307,291), F(288,308,292); and TM7 M(311), A(334), M(315), mostly having their counterparts in other GPCRs from the rhodopsin family. The cleft is big enough to accommodate the AVP pressin ring [34, 39] and the OT tocin ring [40]. In view of the extensive sequence homologies both between OT and VP and their receptors, it is reasonable to assume common or largely similar docking modes for the hormones and antagonists in all their receptors [34, 41, 42]. Hence, in all three receptors we assumed an equivalent active space potentially available to the YM087 ligand including, at the same time, the whole cavity described above. Such assumption was simultaneously in agreement with a common view that small non-peptide ligands completely penetrate an interior of the receptor [14–18]. Simultaneously, it was hoped that random docking-simulated annealing-molecular dynamics could reflect a whatever correlation between ligand arrangements in the receptor models and their biological efficacy.

Receptor-YM087 complexes

The active space for YM087 docking was defined as shown in Methods and the sets of representative structures of the CSA-relaxed and energy-minimized complexes were obtained, see Figure 5. Of 5, 8 and 5 lowest-energy configurations obtained for V2R-YM087, V1aR-YM087, and OTR-YM087 complexes, respectively, 3 per each receptor type, which were selected for subsequent constrained MD, are marked bold in Table 1 and referred accordingly below.

The MD trajectories for these total nine systems are shown in Figure 6. It is seen that until start of the release of the TM Ca positional constraints at 100 ps (cf. Methods) the overall motion of the proteins is severely hampered, except the tips of the N-termini and the centers of the longest IL2 and IL3 loops. Following the gradual release of these constraints between 100–160 ps, all extra- and intracellular loops, also including the effective IL4 between the TM7 C-terminus and the (palmitoyl-Cys)$_2$ sequence, start to move vigorously to get apparently equilibrated at slightly less than 200 ps in the OTR complexes to around 260–270 ps in the V1aR(20) and V2R(06) complexes, see Figure 6. It is also seen that the V2R and OTR complexes exhibit relatively steady and regular motional characteristics, the facts also reflected in the RMS values around 2.1–2.4 Å and 2.5–2.6 Å, respectively, while the V1aR(18) and V1aR(20) look quite stormy between 165–230 ps and 165–250 ps, respectively (see Figure 6-medium), followed past these periods at last by steady dynamical characteristics yet concerning more distorted bundles, reflected in the RMS values around 2.8–2.9 Å. In all trajectories all helices, except the most nested TM3, are here and there displaced and/or distorted, e.g., the most exposed TM1 and TM4 in V2R(26), V1aR(18), OTR(01), OTR(06), OTR(14) and V2R(18), V1aR(18), respectively. Other helices displace and/or distort more sporadically, like TM2 N-terminus in OTR(14), TM5 in V1aR(20) (C-terminus), OTR(14) (center) and TM6 in V1aR(10) and V1aR(18), and TM7 in V2R(26) and OT(14) (C-terminus). These TM receptors motions are correlated with the accompanying motions of the YM087 ligand and doubtless reflect a simulated mutual fitting. Thus, it is seen that most 'stormy' MD trajectories for the V1aR(18) and V1aR(20) complexes, reflect also the largest YM087 replacements in MD (compare Figures 6-medium and 7B) while the most tempered V2R trajectories are associated with only minute ligand motions during MD (compare Figures 6-top and 7A).

The selected MD-equilibrated receptor-ligand complexes are shown and compared in Figure 8. It is seen, that although mutually interfering, the intra-receptor spatial domain accepting YM087 in V2R and V1aR is common and only partly overlapping with that typical of the ligand in OTR. The former is by ca. 2 helical turns closer the extracellular domain than the latter and closely sticking to TM5 and TM6. Accordingly, the latter extends deeper into the receptor cavity and simultaneously is concentrated closer to TM3-TM2-TM7 wall, see Figure 8. The sets of TM5, TM6, TM7 (top) residues and TM3, TM2 and TM7 (bottom) residues, mainly exposed for potential interactions either with the V1aR/V2R-docked ligand cluster or with the OTR-docked ligand cluster, respectively, are detailed in the Figure 8 legend. Some of them are different in the two groups of the receptors, e.g. (V2R vs. OTR) TM5 R203 – K198, V206 – I201, TM3 M120 – V120 and S127 – T127, and these may be primary candidates for conferring V1aR/V2R vs. OTR selectivity.

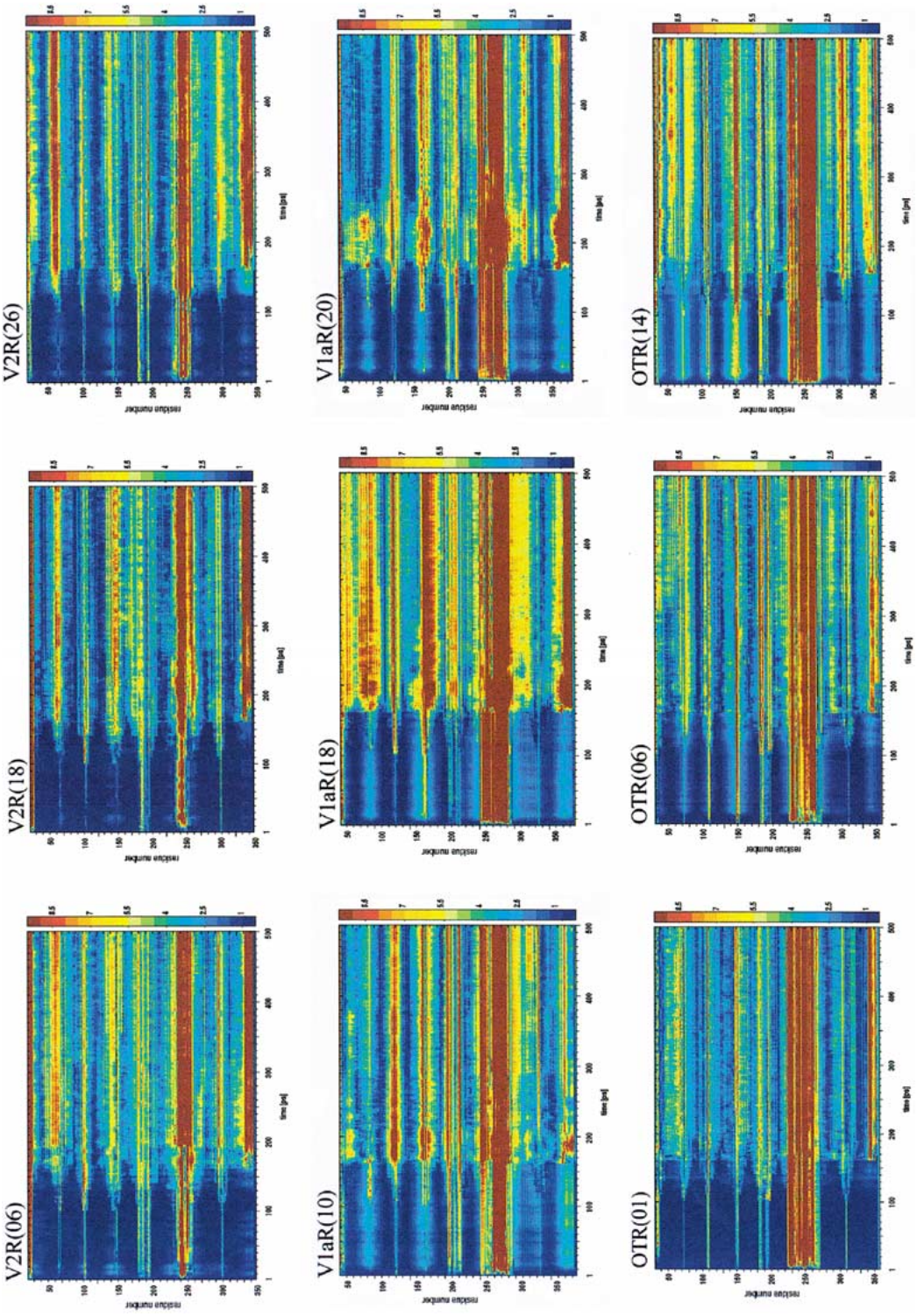

Figure 6. MD trajectories for the selected 9 receptor-YM087 complexes. The RMS values (Å), relative to starts, have been computed using TM helical 15 central C^{α} carbons (105 total) per each configuration, top: V2R(06) 2.42, V2R(18) 2.09, V2R(26) 2.44; medium: V1aR(10) 2.41, V1aR(18) 2.95, V1aR(20) 2.80; bottom: OTR(01) 2.66, OTR(06) 2.52, OTR(14) 2.58.

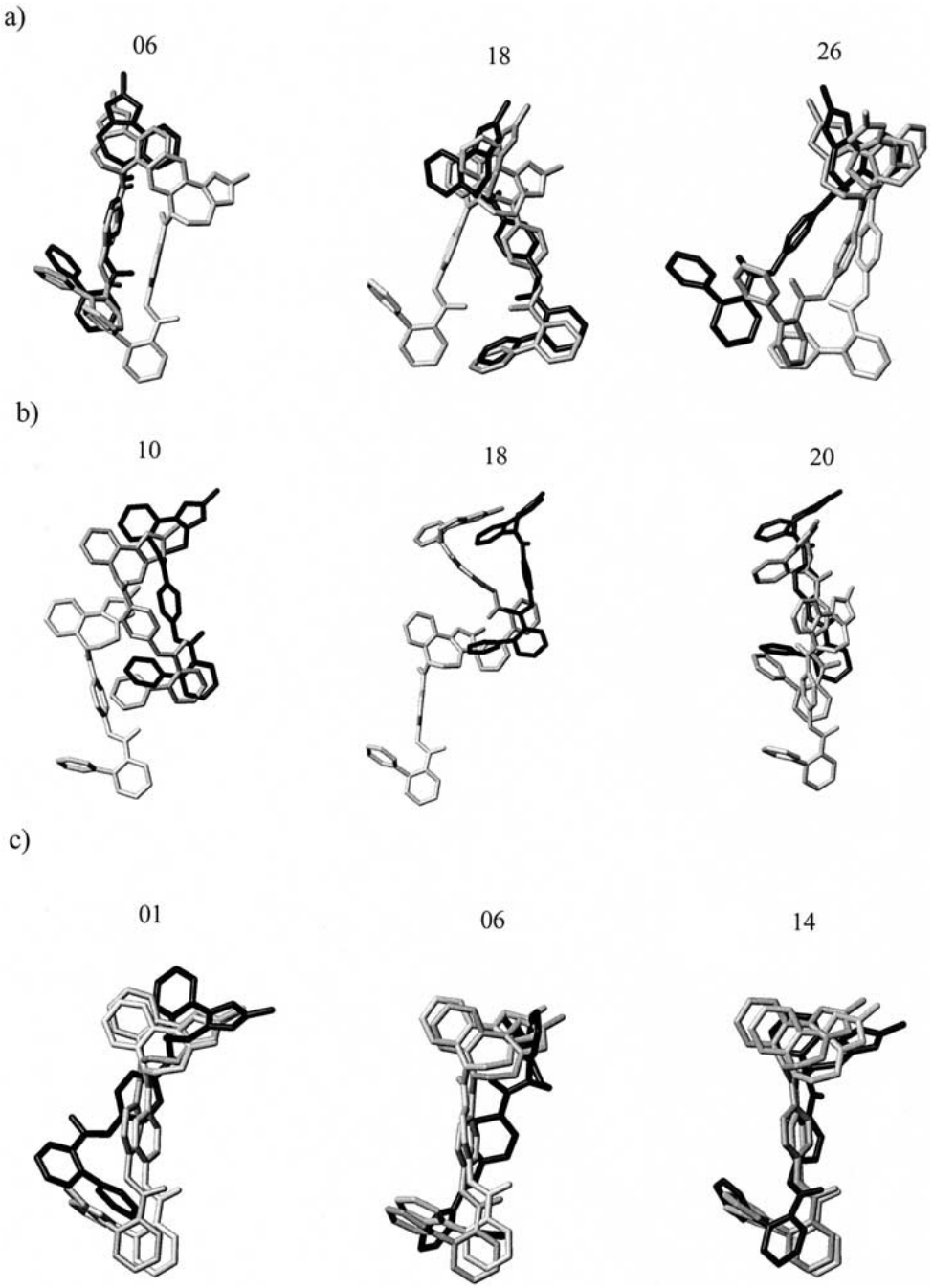

Figure 7. Starting (light), intermediate, after CSA, (gray) and relaxed (dark) YM087 configurations, three per each receptor, for A: YM087-V2R; B: YM087-V1aR; C: YM087-OTR. The diagrams were obtained via optimal superimpositions of the TM domains of the respective starting-intermediate-relaxed triads of each selected receptors-ligand configuration, so that the specific triplets illustrate the extent of motion experienced by a docked YM087 during CSA (light to gray) and MD relaxation (gray to dark).

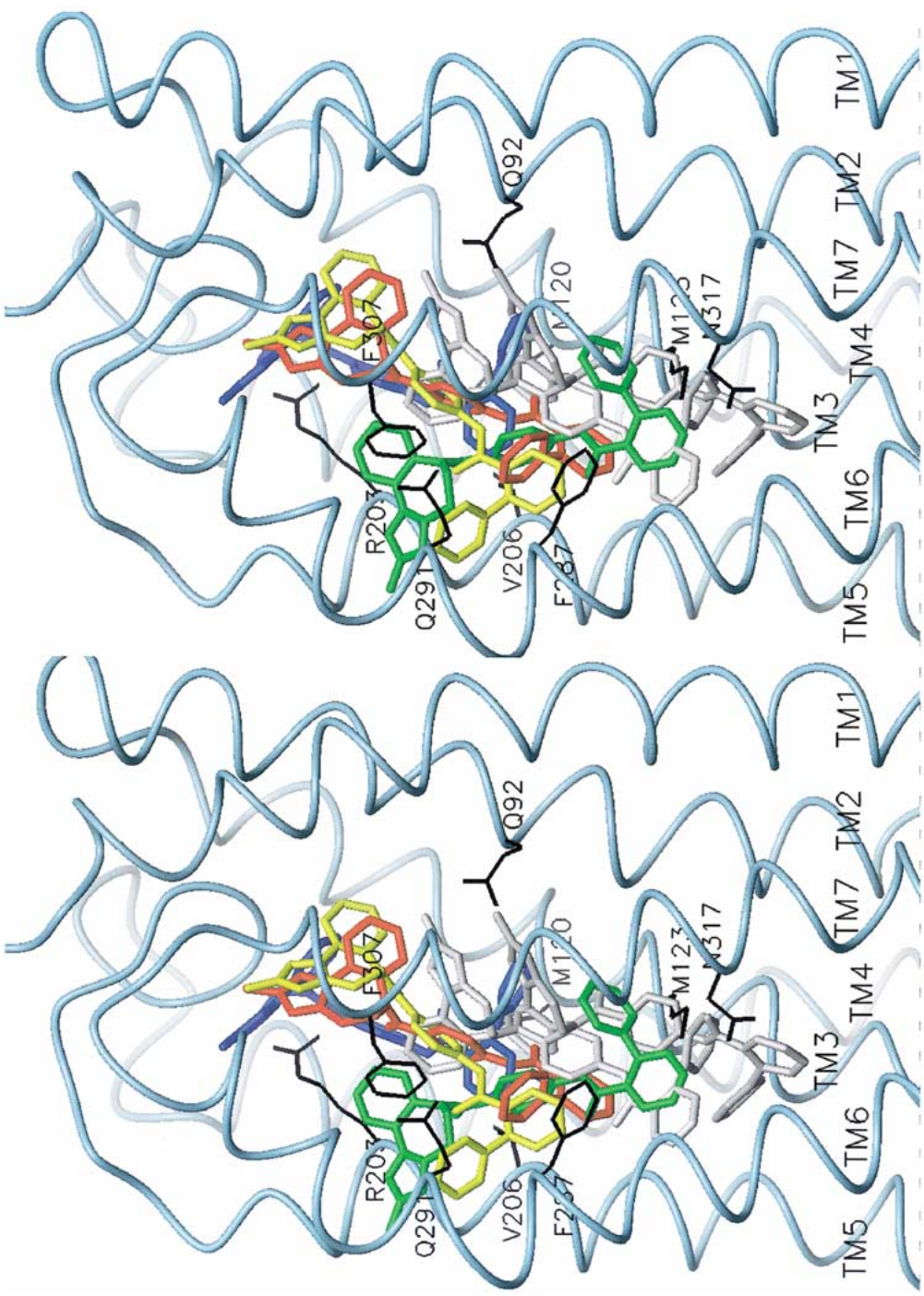

Figure 8. Comparison of the relaxed ligand positions in the optimally overlaid V2, V1a and OT receptors. Since dispersion of the receptors shapes is small (see RMS values in Figure 6), for clarity merely V2R(18) trace is shown as the sky blue backbone rope. The ligands docked in V2R and V1aR (4 of 6, for clarity) are colored while those docked in OTR (2 of 3, for clarity) are gray shaded. It is seen that, despite noticeable dispersion, the ligands docked in V2R and V1aR assemble, on the average, near TM5, TM6 and TM7 top while those docked in OTR prefer, on the average, the opposite side made by TM3, TM2 and TM7 bottom. Selected TM5, TM6 and TM7-top V2R/V1aR residues, not more than 4 Å away of a ligand, are exposed and labeled: TM5 R203/R214, V206/V217, TM6 Q291/Q311), F287/F307, TM7 F307(I330). Similarly exposed are selected TM3, TM2 and TM7 OTR residues (whose actually rendered V2R equivalents follow in parentheses): TM3 V120(M120), M123(M123), T127(S127), TM2 Q92(Q92), TM7 A318(A314), not shown, N321(N317) and S322(S318), not shown.

Receptors and their docking modes

Numerous neurophyseal (V1a, V2 and/or OT) receptor simulations have been done in the past [32, 33, 39, 41–46] prevailingly using reasonably convincing low-resolution structure of rhodopsin [22, 23] or its refined version(s) [20, 24] as template(s). Based on the general agreement between molecular modeling and mutagenesis studies, a concensus is accepted according to which, the native hormones oxytocin and/or vasopressin and their agonist peptide analogs dock their tocin/pressin ring(s) completely nested in the receptor interior, made of a floor of TM3, TM5, TM6 conservative residues and surrounding TM2-TM7 internal walls, while their C-terminal tail(s) interact via their R8(VP)/L8(OT) 'message' residues with EL1 D103/Y115/F103 (in V2R/V1aR/OTR, respectively) [39, 43, 45]. Similarly, it is commonly accepted a view that small-molecule non-peptide antagonists dock entirely in the receptor interior [44, 46] and that they 'freeze' inactive receptor form(s), definitely different from the activated ones [32, 33]. In our view, the recently published first high-resolution structure of dark rhodopsin with 11-*cis*-retinal [21] provides an excellent GPCR template for a general receptor-antagonist complex, just like still unknown meta-II-rhodopsin form with 11-*trans*-retinal would possibly provide the most reliable template for a general receptor-agonist complex [47]. As the model we have used has remembered most closely of all theoretical templates the rhodopsin experimental structure (see above) we hope, that its choice as a start for simulations aimed at antagonist docking, is justified. In the future, we are going to switch to the most reliable experimental template [21] (Figure 2, see also Table 2). In this context, we also believe that the sets of intra-TM bundle interactions between mainly conservative residues, singled-out and proved in this work to be very similar in this model(s) and that relying on the experimental rhodopsin (Tables 2–4), may be of potential use and significance in discussing general mechanisms of GPCR inactivation by antagonists.

Regarding YM087 selectivity, we have shown (see Figure 8) that the domains of its docking within V1aR/V2R against OTR, although partly overlapping, are distinctly shifted relative each other. Specific and non-equivalent sets of amino acid residues were singled out as responsible for the V1aR/V2R-YM087 interaction on the one hand and for OTR-YM087 interaction, on the other (see Figure 8). These features well correlate with the affinity results, which are equal to (K_i, nM) 3.4, 0.48 and 44.4 for V2R, V1aR and OTR (in vitro rat kidney, liver and uterus tissue, respectively) [48]. Thus, the interaction model as a working hypothesis for its experimental testing via mutagenesis-affinity study is provided.

Acknowledgements

We acknowledge professor Henry I. Mosberg of University of Michigan, Ann Arbor, USA for making the G Protein-Coupled Receptor templates available for public use. This work was supported by the Polish Scientific Research Committee (KBN) grants 0752/P04/99/17, 1439/T09/2001/21 and BW/8000-5-0196-1; by the Academic Computer Center in Gdansk TASK, Poland; and by the Interdisciplinary Center for Mathematical Modeling (ICM) in Warsaw, Poland.

References

1. Jard, S., Elands, J., Schmidt, A. and Barberis, C., In Imura H. and Shizurne. K. (Eds.) Progress in Endocrinology, Excerpta Medica, Amsterdam, 1988, pp. 1183–1188.
2. Barberis, C. and Tribollet, E., Critical Rev. Neurobiol., 10 (1996) 119.
3. Freidinger, R.M. and Pettibone, D.J., Med. Res. Rev., 17 (1997) 1.
4. Manning, M. and Sawyer, W.H., J. Lab. Clin. Med., 114 (1989) 617.
5. Serradeil-Le Gal, C., Wagnon, J., Garcia, C., Lacour, C., Guiraudou, P., Chrostophe, B., Villanova, G., Nisato, D., Maffrand, J.P., Le Fur, G., Guillon, G., Cantau, B., Barberis, C., Trueba, M., Ala, Y. and Jard, S. J., Clin. Invest., 92 (1993) 224.
6. Yamamura, Y., Ogawa, H., Chihara, T., Kondo, K., Onogawa, T., Nakamura, S., Mori, T., Tominaga, M. and Yabuuchi, Y., Science, 252 (1991) 572.
7. Serradeil-Le Gal, C., Lacour, C., Valette, G., Garcia, G., Foulon, E., Galindo, G., Bankir, L., Pouzet, B., Guillon, G., Barberis, C., Chicot, D., Jard, S., Vilain, P., Garcia, C., Marty, E., Raufaste, D., Brossard, G., Nisato, D., Maffrand, J.P., and Le Fur, G., J. Clin. Invest., 98 (1996) 2729.
8. Yamamura, Y., Ogawa, H., Yamashita, H., Chihara, T., Miyamoto, H., Nakamura, S., Onogawa, T., Yamashita, T., Hosokawa, T., Mori, T., Tominaga, M. and Yabuuchi, Y., Br. J. Pharmacol., 105 (1992) 787.
9. Freidinger, R.F., Bock, M.G., Evans, B.E., Pettibone, D.J. and Williams, P.D. In Shimonishi, Y. (Ed.), Peptide science – present and future. Proceedings of the 1st International Peptide Symposium, Kyoto 30.11-5.12.97, Kluwer Acad. Publishers, Dordrecht, 1999, pp. 618–622.
10. Yatsu, T., Tomura, Y., Tahara, A., Wada, K., Tsukada, J., Uchida, W., Tanaka, A. and Takenaka, T., Eur. J. Pharm., 321 (1997) 225.
11. Matsuhisa, A., Taniguchi, N., Koshio, H., Yatsu, T., Tanaka, A., Chem. Pharm. Bull, 48 (2000) 21.

12. Pisvanis, J., Naitoh, M., Johnston, C.I., Burrel, L.M., Eur. J. Pharmacol., 381 (1999) 23.
13. Guderman, T., Neunberg, B. and Schultz, G., J., Mol. Med. 73 (1995) 51.
14. Wess, J., FASEB J., 11 (1997) 346.
15. Ji, T.H., Grossman, M. and Ji, I., J. Biol. Chem., 273 (1998) 17299.
16. Gether, U. and Kobilka, B.K., J. Biol. Chem., 273 (1998) 17979.
17. Bikker. J,A., Trumpp-Kallmeyer, S. and Humblet, C., J. Med. Chem. 41, (1998) 2911.
18. Ulloa-Aguirre, A., Stanislaus, D., Janovick, J.A. and Conn, P.M., Archiv. Med. Res., 30 (1999) 420.
19. Baldwin, J.M., EMBO J., 12 (1993) 1693.
20. Baldwin, J.M., Scheltler G.F.X., and Unger, V.M., J. Mol. Biol., 272 (1997) 144.
21. Palczewski, K., Kumasaka, T., Hori, T., Behnke, C.A., Motoshima, H., Fox, B.A., Le Trong, I., Teller, D.C., Okada, T., Stenkamp, R.E., Yamamoto, M. and Miyano, M. Science 289 (2000) 739.
22. Schertler, G.F.X. and Hargrave, P.A., Proc. Natl. Acad. Sci., 92 (1995) 11578.
23. Unger, V.M. Hargrave, P.A. Baldwin, J.M. and Schertler, G.F.X., Nature, 389 (1997) 203.
24. Herzyk, P. and Hubbard, R.E., Biophys. J., 69 (1995) 2419.
25. Peitsch, M.C., Herzyk,P., Wells, T.N.C. and Hubbard, R. Automated G protein-coupled receptor modeling at Swiss-model, http://expasy.hcuge.ch/swissmod/SWISS-MODEL.html
26. Iismaa, T.P., Biden, T.J. and Shine, J. G Protein-Coupled Receptors, Springer-Verlag, Heidelberg, 1995, Chapter 1.
27. Pogozheva, I.D., Lomize, A.L. and Mosberg, H.I., Biophys. J., 70 (1997) 1963.
28. Pogozheva, I.D., Lomize, A.L. and Mosberg, H.I., Biophys. J., 75 (1998) 612.
29. Morris, G.M., Goodsell, D.S., Huey, R. and Olson, A.J., J. Comput. Aid. Mol. Des., 10 (1996) 293.
30. AMBER 5.0, Case, D.A., Pearlman, D.A., Caldwell, J.W., Cheatham III, T.E., Ross, W.S., Simmerling, C., Darden, T., Merz., K.M., Stanton, R.V., Cheng, A., Vincent, J.J., Crowley, M., Ferguson, D.M., Radmer, R., Seibel, G.L., Singh, U.C., Weiner, P.K. and Kollman, P.A. (1997) AMBER, v.5.0, University of California, San Francisco, CA, U.S.A.
31. SYBYL 6.1 (1994) Tripos Inc., 1699 S. Hanley Rd., St. Louis, MO 63144, USA.
32. Fanelli, F., Barbier, P., Zanchetta, D., De Benedetti, P.G. and Chini, B., Mol. Pharmacol., 56 (1999) 214.
33. Scheer, A., Fanelli, F., Costa, T., De Benedetti, P.G. and Cotecchia, S., EMBO J., 15 (1996) 3566.
34. Czaplewski, C., Kazmierkiewicz, R. and Ciarkowski, J., J. Comput. Aid. Mol. Design, 12 (1998) 275.
35. Schmidt, M.W., Baldridge, K.K., Boatz, J.A., Elbert, S.T., Gordon, M.S., Jensen, J.H., Koseki, S., Matsunaga, N., Nguyen, K.A., Su, S., Windus, T.L., Dupuis, M. and Montgomery, J.A., J. Comput. Chem., 14 (1993) 1347.
36. Bayly, C.I, Cieplak, P., Cornell, W.D. and Kollman, P., J. Phys. Chem., 97 (1993) 10269.
37. Koradi, R., Billeter, M., and Wüthrich, K., J. Mol. Graphics, 14 (1996) 51.
38. Corpet, F., Nucl. Acids Res., 16 (1988) 10881.
39. Mouillac, B., Chini,B., Balestre, M.-N., Elands, J., Trumpp-Kallmeyer,S., Hoflack,J., Hibert,M., Jard,S. and Barberis C., J. Biol. Chem., 270 (1995) 25771.
40. Politowska, E., Czaplewski, C. and Ciarkowski, J., Acta Biochim. Pol., 46 (1999) 581.
41. Czaplewski, C, Kazmierkiewicz, R. and Ciarkowski, J., Acta Biochim. Pol., 45 (1998) 19.
42. Czaplewski, C, Kazmierkiewicz, R. and Ciarkowski, J., Lett. Peptide Sci. 5 (1998) 333.
43. Hibert, M., Hoflack, J., Trumpp-Kallmeyer, S., Mouillac, B., Chini, B., Mahé, E., Cotte, N., Jard, S., Manning, M. and Barberis, C.J., Rec. Signal Transd. Res., 19 (1999) 589.
44. Cotte, N., Balestre, M.-N., Aumelas, A., Mahé, E., Phalipou, S., Morin, D., Hibert, M., Manning, M., Durroux, T., Barberis, C. and Mouillac, B. Eur. J. Biochem., 267 (2000) 4253.
45. Chini,B., Mouillac, B., Ala, Y., Balestre, M.-N., Trumpp-Kallmeyer,S., Hoflack,J., Elands, J., Hibert,M., Manning, M., Jard,S. and Barberis C., EMBO J., 14 (1995) 2176.
46. Thibonnier, M., Coles, P., Conarty, D.M., Plesnicher, C.L. and Shoham, M.J., Pharmol. Exp. Ther., 294 (2000) 195.
47. Babak, B., Souto, M.L., Imai, H., Shichida, Y. and Nakanishi, K., Science, 288 (2000) 2209.
48. Tahara, A., Tomura, Y., Wada, K.I., Kusayama, T., Tsukada, J., Takanashi, M., Yatsu, T., Uchida, W. and Tanaka, A., J. Pharmacol. Exp. Ther., 282 (1997) 301.